Entanglements and Dynamics of Polymer Melts near a SWCNT

ARTICLE *in* MACROMOLECULES · SEPTEMBER 2012

Impact Factor: 5.8 · DOI: 10.1021/ma3007637

Macromolecules

Article

pubs.acs.org/Macromolecules

Entanglements and Dynamics of Polymer Melts near a SWCNT

Argyrios Karatrantos,[†] Russell J. Composto,[‡] Karen I. Winey,[‡] Martin Kröger,[§] and Nigel Clarke*,[†]

[†]Department of Physics and Astronomy, University of Sheffield, Sheffield S3 7RH, United Kingdom

[‡]Department of Materials Science and Engineering, University of Pennsylvania, Philadelphia, Pennsylvania 19104, United States

[§]Polymer Physics, Department of Materials, ETH Zurich, CH-8093 Zurich, Switzerland

ABSTRACT: We investigate the topological constraints (entanglements) and dynamics of monodisperse polymer melts in the presence of a single wall carbon nanotube (SWCNT) in comparison to inclusion-free polymer melts by molecular dynamics simulations. The SWCNT has an infinite aspect ratio and radius smaller than the polymer radius of gyration. In the presence of SWCNT with or without attractive interactions, the contour length of the primitive path increases indicating more entanglements. We also find that there is a large heterogeneity in the polymer dynamics due to the polymers in contact with the SWCNT. The overall polymer diffusion decreases compared to its melt value and is affected by the enthalpic interaction between monomeric units and SWCNT, and the SWCNT radius. Moreover, the polymer chain diffusivity perpendicular to SWCNT is less than that parallel to the SWCNT in the entangled polymer systems where there is attraction between polymers and SWCNT surface. In the absence of SWCNT-polymer attractions, the polymer diffusion retains its melt value.

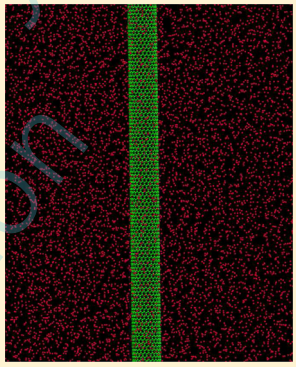

I. INTRODUCTION

Experimental studies of polymer/single wall carbon nanotubes (SWCNT) nanocomposites have focused on the electrical, thermal, structural, and rheological properties;[1−11] however, to the best of our knowledge, very few studies have addressed the dynamic properties[7,8,12] in a polymer/SWCNT nanocomposite system. Understanding the polymer dynamics of such systems is very important from a technological point of view, more specifically for the optimization of the design of fabrication methods for nanocomposites. Recently it was shown that the addition of SWCNTs initially suppresses polymer diffusion, and then beyond the percolation threshold the diffusion recovers.[7] Remarkably, this behavior is observed only when the polymer radius of gyration is larger than the nanotube radius.[8] One objective of this paper is to better understand the dynamics underlying macromolecule diffusion in polymer/SWCNT nanocomposites.

For pure polymer melts, the diffusion of long polymer chains of molecular weight M into matrices is independent of the matrix molecular weight, P, for sufficiently large P above a critical value P_c.[13−16] The diffusion coefficient follows the scaling relation $D_0 \propto M^{-2}$, in agreement with the Doi−Edwards model of chain reptation.[17] Moreover, it was well observed that when the matrix molecular weight is similar to or less than that of the diffusing polymers, there is an additional contribution to the polymer chain diffusion due to the constraint release process[18] that depends on the matrix molecular weight, following the scaling relation $D_0 \propto M^{-1}P^{-3}$;[13−16] the result is an enhanced polymer chain diffusion. More recent measurements of polymer chain self-diffusion contradict the widespread idea that in polymer melts $D_0 \propto M^{-2}$ and demonstrate that for different polymers such as polystyrene, polybutadiene, and poly(dimethyl siloxane) the diffusion coefficient follows the relation $D_0 \propto M^{-2.28}$.[19] In addition to the experimental studies,[13−16,19] monodisperse polymer melts have also been investigated by means of molecular simulation, using bead spring molecules (chains) interacting only with excluded volume interactions.[20,21] The dynamic properties of such polymer melt models have successfully predicted the scaling laws for both unentangled[16,22,23] and entangled polymer melts.[13−17,22,23]

A few simulation studies have been undertaken on the dynamics of polymers loaded with spherical,[24−38] cylindrical,[39,40] icosahedral,[41,42] X- and Y-shaped[43] nanoparticles. It was found that polymer chain diffusivity is enhanced, relative to its bulk value, when polymer−particle interactions are repulsive,[26,28] specifically up to 20% near a spherical nanoparticle surface. However, when polymer−particle interactions are attractive,[26,28−31,37,38,42] the dynamics of the interfacial polymers are strongly perturbed by the nanoparticles,[26,32,37,38,42] so that the diffusivity of entangled polymers is reduced, in particular, by ∼40% near a spherical nanoparticle surface.[28] The role of attractive interactions in polymer chain dynamics was explored further[31,36] showing that a weak attraction with a spherical nanoparticle does not influence the chain diffusivity; instead, above a critical value of the energy gained during attraction, the chain diffusivity gradually decreases to zero.[31] Furthermore, an anisotropy was observed near the nanoparticle in the polymer chain diffusivity.[25] Most notably, in the direction normal to the spherical nanoparticle the chain diffusivity is lower than in the direction tangential to the nanoparticle.[25] Additionally, the dynamics of the polymer

Received: April 14, 2012
Revised: July 31, 2012
Published: August 24, 2012

   dx.doi.org/10.1021/ma3007637 | *Macromolecules* 2012, 45, 7274−7281

chains can be slowed down by geometric effects such as the confinement caused by the spherical nanoparticles.[29] Anomalous diffusion in which the polymer chain motion exhibits a subdiffusive regime followed by a normal Fickian diffusion has recently been found.[33,36] Another factor that alters the overall polymer diffusion behavior is the nanoparticle concentration,[28,31,34] where in the case of repulsive spherical nanoparticles, the polymer chain diffusion coefficient, although initially increasing with nanoparticle concentration, finally reduces at large volume fractions of nanoparticles.[28] In contrast, in the case of strongly nanoparticle−polymer attraction, the overall polymer chain diffusion decreases linearly with the increase of spherical nanoparticle concentration.[28,31,34]

The aforementioned studies have investigated the effect of spherical nanoparticles on polymer diffusion, while it is recognized[38,44,45] that the polymer dynamics is strongly influenced by the characteristics of the nanoparticles (e.g., size, shape, aspect ratio, type of nanoparticle surface, volume fraction of nanoparticles) and the polymer (e.g., molecular weight, structure, nature of the interactions between the nanoparticle and the polymer matrix). Thus far only atomistic simulations[46−50] have been applied to the polymer dynamics in the vicinity of SWCNT. Specifically, the role of the interaction between polyethylene oligomers and SWCNTs on the chain diffusivity has been explored by small sized atomistic simulations.[46,47] In particular, an increase in the diffusion coefficient is observed (it is questionable though if the diffusive regime has been reached) in polyethylene oligomer−SWCNT composites[46] comparative to the polyethylene melt above the glass transition, in contrast to previous studies of systems with spherical nanoparticles.[25,32]

In this paper, we provide a systematic simulation study which shows how the interaction between polymer chains and SWCNT, and the radius of the SWCNT, affect the entanglements of polymer chains and the diffusion of polymer chains in the vicinity of, and at a distance from, a single nanotube. We utilize a coarse grained model of flexible polymers,[51] with the SWCNT considered at the atomistic level. This extends our recent simulation of chain structure in the presence of a SWCNT in which we found that the local structure of the chains is significantly affected by the nanotube although the overall configuration as reflected in the radius of gyration was unperturbed.[52] The rest of this paper is organized as follows. In Section II, we present the general features of the simulation methodology, the simulation details that were used to investigate the entanglements and dynamics of polymer melts with a SWCNT, the different estimators that can calculate the topological constraints (entanglements) of polymer systems, and the theoretical background for the dynamic properties. In Section III, we consider monodisperse polymer melts with a SWCNT in the simulation cell. In particular, we performed a topological analysis and calculated the entanglements, using different estimators, for polymer melts in the presence of the SWCNT and compare with that of the inclusion-free polymer melts. Furthermore, we investigate the dynamics of the polymers that are in contact with, in the vicinity of, and at distance from the SWCNT at different interaction strengths and various radii of SWCNT. Finally, in Section IV, conclusions are drawn from the study.

II. SIMULATION METHOD

We performed molecular dynamics (MD) simulations of monodisperse polymer melts and monodisperse polymer melts with a SWCNT.[52] The polymer melt is simulated by using a coarse grained polymer model motivated by the work of Peter et al.[51] and Bennemann et al.[53] Polymer chains are composed of bead−spring chains of Lennard−Jones (LJ) monomers m of diameter $\sigma_m = 1$ and mass $m_m = 1$. The radius of a SWCNT is of the order of the Kuhn length of polystyrene (PS). In these simulations an atomistic model was used for the SWCNT. Since the polymer model used is coarse grained, the monomer-carbon interaction cannot be captured at the atomistic level. However, by using an atomistic SWCNT and a coarse grained polymer model for different ϵ_{mc} values we can select polymers interacting differently with the SWCNT surface. Three different SWCNTs (12,0), (17,0), (22,0) of radius $r_{SWCNT}/\sigma_m = 0.46, 0.66, 0.85$, respectively, are considered. Each SWCNT spans the simulation cell with its atoms held fixed in a centered position in the simulation cell and is oriented along the z axis.

Nonbonded monomer−monomer as well as monomer (m)-carbon (c) interact via a truncated and shifted Lennard−Jones (LJ) potential,[54,55] with a cutoff radius $r_c = 2.3\sigma_m$, given by[56−59]

$$U_{LJ}(r_{ij}) = \begin{cases} 4\epsilon\left[\left(\frac{\sigma_{ij}}{r_{ij}}\right)^{12} - \left(\frac{\sigma_{ij}}{r_{ij}}\right)^{6} - C(r)\right] & \text{for } r < r_c \\ 0 & \text{for } r_c \geq r \end{cases} \quad (1)$$

where $C(r)$[56−59] is a third degree polynomial which is included so that the potential vanishes continuously at $r = r_c$, ϵ is a characteristic interaction energy (interaction strength) between particles, and r_{ij} is the distance between particles i and j. The interaction energy between monomers is $\epsilon_{mm} = k_BT = 1$ (where k_B is Boltzmann's constant and T is temperature). The distance between neighboring carbon atoms in the SWCNT is $\sigma_c = 0.141$. For the monomer−carbon interaction, we use a geometric mean combination rule: $\sigma_{mc} = (\sigma_m \times \sigma_c)^{1/2} = (0.141 \times 1)^{1/2} \approx 0.3755$. The nature of the polymer-SWCNT interactions is defined by the interaction energy between monomer and carbon, ϵ_{mc} which varies between 0−1 k_BT. For the simulations where the polymers have no attractive interaction with the nanotube surface, only the repulsive term of eq 1 is retained and in order to have a very slight repulsion, $\epsilon_{mc} = 5 \times 10^{-4} k_BT$ (we will refer to this case as $\epsilon_{mc} = 0$). The case of $\epsilon_{mc} = 0$ resembles repulsive nanoparticles. The case of $\epsilon_{mc} = 0.5k_BT$ denotes a weak interaction between monomers and carbon (in atomistic simulations of polyethylene-SWCNT, $\epsilon_{mc} = 0.461$ KJ/mol[46] or $\epsilon_{mc} = 0.449$ KJ/mol[50,60]). The case of $\epsilon_{mc} = 1k_BT$ resembles attractive nanoparticles which can be miscible and well dispersed in a polymer matrix. When there is an attraction between polymers and SWCNT surface ($\epsilon_{mc} = 1k_BT$) the distance where $U_{LJ} = 1k_BT$ is: $r \approx 0.97\sigma_{mc} \approx 0.364\sigma_m$. The monomer number density around this distance has been calculated in ref 52.

For nearest-neighbor monomers along the chain the LJ interaction is not included. Technically, these monomers are connected to each other by a harmonic bond potential,[51,61] given by

$$U_{bond}(r) = \frac{K}{2}(r - r_0)^2 \quad (2)$$

with an equilibrium bond length $r_0 = 0.967\sigma_m$ and a spring constant $K = 1111\epsilon_{mm}$.[51,61] The value of K is large enough to

prevent the chains from cutting through each other in the simulation, to allow the formation of entanglements.

A. Simulation Details. In this study, *NVT* molecular dynamics simulations were performed using the GROMACS package[56−59] at a melt density $\rho^* = (N_m/V)\sigma_m^3 = \rho\sigma_m^3 = 0.85$ (where N_m is the total number of monomeric units in the system, and V is the volume of the polymer melt). In any simulation of the polymer melts with a SWCNT, one SWCNT was inserted in the simulation cell, and the volume of the simulation cell was increased according to the volume of the SWCNT (not the excluded volume of the SWCNT). By doing this and considering the small volume fraction of the SWCNT we expect that the monomer number density, and total free volume, is the same with that of the melt. That simulations were performed at filler volume fraction of 0.4% in accordance with a recently studied PS/SWCNT nanocomposite.[7,8] The length of the simulation cell was always larger than the end-to-end distance of the polymer chains. To set the temperature at $T^* = k_BT/\epsilon = 1$, the Nose-Hoover[62,63] thermostat was used with an oscillation relaxation constant $\tau_T = 2.0\tau$. The equations of motion were integrated using the leap−frog-algorithm[64] with a time step equal to 0.005τ, where $\tau = (m\sigma_m^2/k_BT)^{1/2}$ is the LJ time unit. Polymer chains with the correct end-to-end distance ($R_{ee}^2 = r_0^2c_\infty(N-1)$, using a characteristic ratio $c_\infty = 1.76$, $r_0 = 0.967$) were inserted randomly into the simulation cell. First the fast push off method was applied.[65] Then extensive MD simulation runs of 60×10^6 steps for $N \geq 50$ and 30×10^6 steps for $N = 10, 30$ were performed to relax the chains. During that time interval the polymers moved several end-to-end polymer distances in the simulation cell. The resulting structures from the above equilibration were used as starting structures for production runs of $30-100 \times 10^6$ steps depending on the length of molecules and system studied. Details (number of polymer chains N_p, number of monomers N in a polymer chain, length of the cubic simulation cell L, self-diffusion coefficient D_0) of the simulated systems are given in Table 1 and the Model Validation section.

Table 1. Simulations of Polymer Melts with a SWCNT[a]

SWCNT	N_t	$L_x = L_y$	L_z
(12,0)	5760	14.431	32.648
(17,0)	5760	18.960	18.923
(22,0)	11520	24.536	22.598

[a]Type of SWCNT, total number of monomers N_t in the simulation cell, and lengths of the simulation cell in the x, y, and z directions ($L_x = L_y$, L_z).

B. Estimators for Entanglement Length N_e. The motion of long chains is limited by entanglements which are topological constraints imposed by the other chains. The number of monomers between entanglements N_e can be calculated by different estimators. The N_e estimator of Everaers et al.[66] (which we denote as "classical S-coil") is determined by statistical properties of the primitive path (shortest path connecting the two ends of the polymer chain subject to the topological constraints) as a whole ('coil') and evaluated for a given N as follows

$$\mathcal{N}_e(N) = (N-1)\frac{\langle R_{ee}^2\rangle}{\langle L_{pp}\rangle^2} \tag{3}$$

where R_{ee} is the end-to-end vector distance of a polymer chain, and L_{pp} is the contour length of its primitive path. The averages are taken over the ensemble of all chains at each single time step. Then the time average is taken for 4000 saved configurations (at a time larger than the disentanglement time, ($t > \tau_e$), in which the polymer chains have diffused an end-to-end distance) for $N < 128$. For $N = 128$, the time average is taken for 1000 saved configurations.

It is known that using the S-coil estimator (eq 3) following,[66] one underestimates N_e. However, it is known that $N_e \equiv \lim_{N\to\infty}\mathcal{N}_e(N)$ (N-independent quantity). In addition, there are modified estimators which provide either an upper bound for N_e or determine N_e from the variation of $\mathcal{N}_e$ with N, cf. ref 67. The "modified S-coil" estimator provides an upper bound to N_e and is given by[67]

$$\mathcal{N}_e(N) = (N-1)\left(\frac{\langle L_{pp}^2\rangle}{\langle R_{ee}^2\rangle} - 1\right)^{-1} \tag{4}$$

To obtain a more accurate N-independent value, we use an ideal N_e estimator ("M-coil")[67] using coil properties

$$\left(\frac{C(x)}{x}\right)_{x=\mathcal{N}_e(N)} = \frac{d}{dN}\left(\frac{\langle L_{pp}\rangle^2}{R_{RW}^2(N)}\right) \tag{5}$$

where $C(x) \equiv \langle R_{ee}^2\rangle/R_{RW}^2(x)$ is the characteristic ratio[22] for a chain with x monomers, and $R_{RW}^2(x) = (x-1)r_0^2$ is the reference square end-to-end distance of a random walk. The derivative of eq 5 means that the $\langle L_{pp}\rangle$ needs to be measured as function of N. In order to obtain an error bar for the N_e values, we solve the "M-coil" estimator again for the lower and upper limits of R_{ee} (end-to-end vector distance) and L_{pp} (contour length of primitive path) as these are extracted from the Z1 algorithm.[67−70]

C. Self-Diffusion Coefficient. The dynamic properties of polymer chains are estimated through the self-diffusion coefficient D_0 which is calculated through the mean square displacement[54]

$$D_0 = \frac{1}{6}\lim_{t\to\infty}\frac{d}{dt}\langle|\mathbf{r}_i(t) - \mathbf{r}_i(0)|^2\rangle \tag{6}$$

where $\langle|\mathbf{r}_i(t) - \mathbf{r}_i(0)|^2\rangle$ is the time dependent displacement of a given atom averaged over time and atoms of the ensemble ($\mathbf{r}_i$ is the position of a monomer i). The self-diffusion coefficient of the polymer chains is calculated in the diffusive regime[54,55] where the mean square displacement increases linearly with time.

III. RESULTS AND DISCUSSION

A. Topological Constraints. Understanding if the SWCNT influences the entanglement length N_e is important because N_e relates changes in the chain structure to rheological properties.[66,71,72] Let us now discuss the entanglement length N_e of the polymer melt in the presence of the SWCNT as determined by the estimators (eqs 3 and 4), evaluated using the geometrical Z1 algorithm.[67−70] We depict the behavior of both estimators ("classical S-coil" and "modified S-coil") in Figure 1. Besides the expected monotonic behavior with respect to variation with N, we observe that for given N, the estimator $\mathcal{N}_e(N)$ decreases in the systems with a SWCNT, compared with the inclusion-free polymer melt either when there is no attractive interaction or an attraction between the polymers and

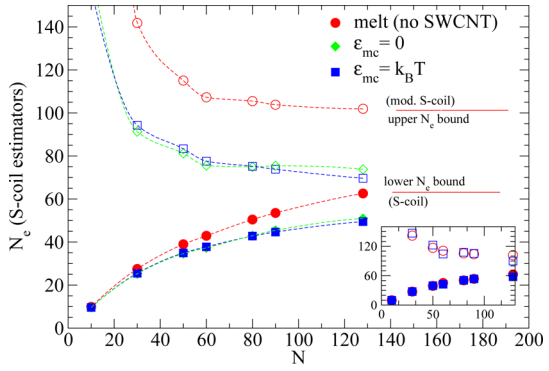

Figure 1. N_e estimated from $N_e(N)$ using eq 3 (S-coil, filled symbols) and eq 4 (modified S-coil, open symbols) for: (i) polymer melts (circles), (ii) polymer melts with a SWCNT (r_{SWCNT} = 0.66) in the absence of attractive interaction between polymers and SWCNT surface (diamonds), (iii) polymer melts with a SWCNT and attractive (k_BT) interaction between polymers and SWCNT surface (squares). Dashed lines interpolating between data points have been added to guide the eye.

SWCNT surface. The upper and lower bound of N_e for a polymer melt are 102 and 62, respectively, as noted by the red lines in Figure 1.

Figure 2 shows the M-coil estimator (eq 5) for all the systems analyzed in Figure 1. For the polymer melt used in this

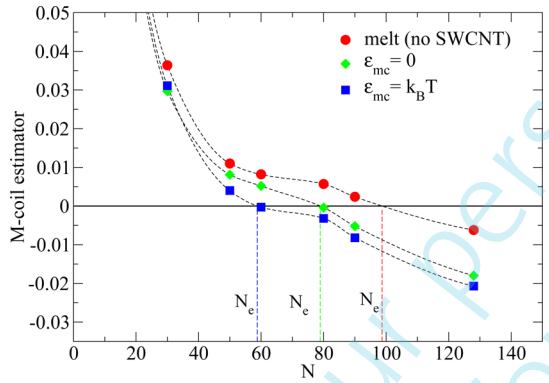

Figure 2. Ne estimated from $Ne(N)$ using eq 5 for polymer melts with a SWCNT (r_{SWCNT} = 0.66) and melts: (i) polymer melts (circles), (ii) polymer melts with a SWCNT in the absence of attractive interaction between polymers and SWCNT surface (diamonds), (iii) polymer melts with a SWCNT and attractive (k_BT) interaction between polymers and SWCNT surface (squares). Dashed lines interpolating between data points have been added to guide the eye.

study $N_e \approx 98.8$ (with a lower limit: 96.3 and an upper limit: 101) from M-coil, and $N_e \in [60,100]$ from the S-coils, which is comparable with previous studies that found $N_e \approx 85$[67,73] (for the LJ+FENE model). Despite large error bars due to the small number of chain lengths studied, Figure 2 shows that N_e decreases in the polymer melt systems with a SWCNT compared to its melt value. The same trend is detected from the measurement of the number of kinks (results not shown). Differences between the Z1 algorithm and the primitive path analysis[66,71] and the difference between N_e estimated from kinks and coils have been discussed previously.[67,69] In particular, recent studies show that polymers in contact with the SWCNT remain unperturbed by either the interaction between the polymer and carbon nanotube surface or by variations in the SWCNT radius, although there is a monomer depletion or a higher monomer density in the vicinity of the carbon nanotube[52] depending on the interaction with the carbon nanotube surface. Thus, the decrease of N_e in the polymer melt with SWCNT (N_e = 78.5, (with a lower limit: 65.2 and an upper limit: 87.2)) is due to the larger contour length of the primitive path, L_{pp}, that is created by the presence of the carbon nanotube. When the SWCNT is removed and replaced with vacancy the polymer−polymer path network is not altered (N_e is that of a polymer melt) as is depicted in the inset of Figure 1. Thus, the decrease of the N_e (increase in entanglement density) in polymer melts with a SWCNT is due to the polymer/SWCNT entanglements.

In addition, when there is an attractive interaction between the polymers and the carbon nanotube surface, the N_e decreases even further (N_e = 58.8, (with a lower limit: 50.3 and an upper limit: 81.9)) due to the higher monomer density[52] in the vicinity of the carbon nanotube. Furthermore, the disentanglement effect does not appear in the vicinity of the carbon nanotube as recently reported for thin polymer films[74] and on a bare flat surface.[75] The disentanglement effect on thin films and on a flat surface is due to the fact that polymers in the vicinity of the surface only have neighboring chains on one side and no chains to entangle with on the other side, thus they have smaller total number of entanglements.

B. Effect of Interaction Strength on Polymer Chain Dynamics. In this section, we will discuss the dynamic behavior of polymer chains in the vicinity of a SWCNT surface for different monomer-SWCNT interaction strengths. First, the case where there is no attractive interaction between polymer chains and SWCNT will be considered. In this case an excluded volume repulsion between the monomers and the carbon atoms of the SWCNT allows consideration of an impenetrable SWCNT. In Figure 3 the self-diffusion coefficient of the polymer chains with a SWCNT, D, scaled with its melt value D_0, is depicted for a different number of monomers per chain. As can be clearly seen, polymer chain diffusion in the presence of a SWCNT is similar to its melt value. Consequently, there is no alteration of the polymer chain diffusivity due to geometric effects when the polymer radius of gyration is greater than the SWCNT radius. Also, in Figure 4, the mean square displacement of polymer chains for N = 30, 60, 128 (black lines) in the polymer melt with a SWCNT system is depicted in two different directions, parallel (z direction) and perpendicular (the average mean square displacement in the x and y directions) to SWCNT. As can be seen, the polymer diffusion is independent of the direction with respect to the SWCNT.

Let us now focus on the case where there is an attractive interaction, modeled by the LJ potential, (eq 1), between polymer chains and SWCNT. In such a case the polymer radius of gyration is not perturbed by the interaction between the polymers and the SWCNT.[52] In Figure 3 we show the self-diffusion coefficient of the polymer chains in the polymer melt with a SWCNT system scaled with its melt value, (D/D_0), for different N. As can be seen, as N increases there is a decrease in the polymer chain diffusivity compared to the melt in the case of entangled polymer melts with a SWCNT. In the case of unentangled polymer (N = 10) with a SWCNT, the polymer chain diffusivity retains its melt value. In order to understand the diffusion behavior of the polymer chains in the presence of the SWCNT we show in the inset of Figure 3 the mean square displacement of the polymer chains that are always "in contact"

dx.doi.org/10.1021/ma3007637 | Macromolecules 2012, 45, 7274−7281

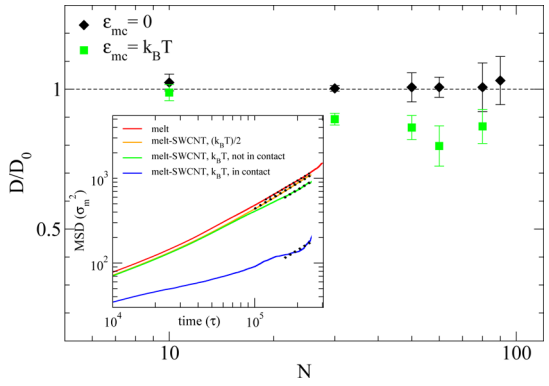

Figure 3. Self-diffusion coefficient of polymers as a function of monomers per chain for a monodisperse polymer melt with a SWCNT (r_{SWCNT} = 0.66) normalized by its melt value: (i) polymer diffusion in a melt with a SWCNT without attractive interaction between polymers and SWCNT (diamonds) and (ii) polymer diffusion in a melt with a SWCNT with attractive interaction ($\epsilon_{mc} = k_BT$) between polymer and (squares). Dashed line has been added to guide the eye. Inset: Mean square displacement of polymer chains for N = 60 i) all polymer chains in the melt without SWCNT (red line), ii) all polymer chains interacting with $k_BT/2$ attraction with the SWCNT (orange line), iii) polymer chains "not always in contact"(detached) from the SWCNT interacting with k_BT attraction (green line), and iv) polymer chains "in contact" with the SWCNT interacting with k_BT attraction (blue line). The dotted lines are linear fitting to the data, showing the diffusive regime.

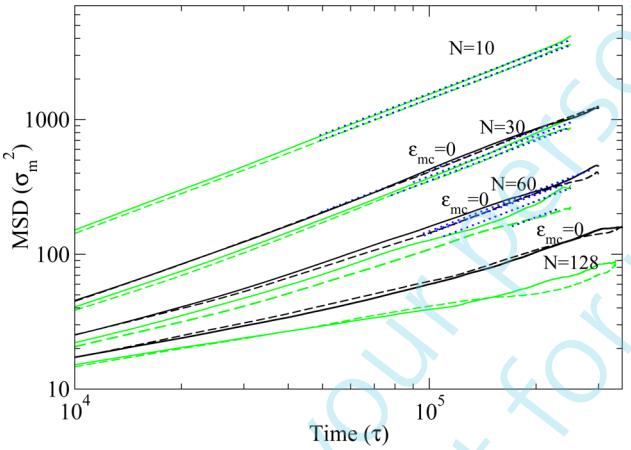

Figure 4. Mean square displacement of polymer chains, with an attractive ($\epsilon_{mc} = k_BT$) interaction (green) parallel (solid lines) and perpendicular (dashed lines) to SWCNT (r_{SWCNT} = 0.66) for four different number of monomers per chain (N = 10, 30, 60, and 128). For comparison we show the MSD for N = 30, 60, and 128 with no attractive interaction with the SWCNT surface (black). The blue dotted lines are linear fitting to the data, showing the diffusive regime. The N = 128 polymers have not reached the diffusive regime.

(polymers that always have monomers that are within a σ_m radial distance from the SWCNT surface during the simulation run, which diffuse around or along the SWCNT) with the SWCNT surface and compare it with the rest of the polymer chains (polymers "not always in contact") and also its melt value (without SWCNT). As can be seen, there is a large heterogeneity in the polymer chain dynamics in the presence of the SWCNT. Additionally, the mean square displacement of the polymer chains (N = 60) that are "not always in contact" with the SWCNT is smaller than its melt value, showing that these polymer chains are influenced by the interaction with the nanotube surface. The depletion or attraction of the polymer to the SWCNT appears at a short distance from the nanotube surface. At an approximately polymer radius gyration, (R_g), distance from the SWCNT surface, the polymer number density is the same to its melt value as was calculating by the monomer-carbon radial distribution function.[52] This is independent of monomers per chain N as suggested by previous simulation and theoretical studies. We expect that any small amounts of extra free volume due to pressure fluctuations would be negligible.

Figure 4 shows the mean square displacement of the polymer chains that have an attractive interaction of k_BT with the SWCNT (green lines) parallel and perpendicular to SWCNT. The polymer chain diffusion depends on the direction with respect to SWCNT. In particular, the polymer self-diffusion coefficient perpendicular (using the average mean square displacements of the x and y direction) to SWCNT, D_{per}, is smaller than that parallel to the SWCNT, D_{par}. This type of dynamic anisotropy, due only to attractive interaction with the nanotube surface, is in qualitative agreement with that observed in simulations of spherical nanoparticle composites.[34] This diffusion anisotropy is smallest for the unentangled polymer (N = 10, 30) melts with a SWCNT $((D_{par} - D_{per}/D_{par})/D_{par} \approx$ 10%, 6% for N = 10 and 30, respectively).

To better understand the decrease of the polymer chain dynamics and diffusion anisotropy that appear in the polymer melt in the presence of the SWCNT, let us now focus on the dynamic behavior of the polymer chains for N = 60, that are in cylindrical shells with radii that are integer multiples of half of the (square root of the mean square) polymer radius of gyration (R_g = 3.886[52]) around the SWCNT, according to the position of the polymer chain center of mass. In Figure 5 we

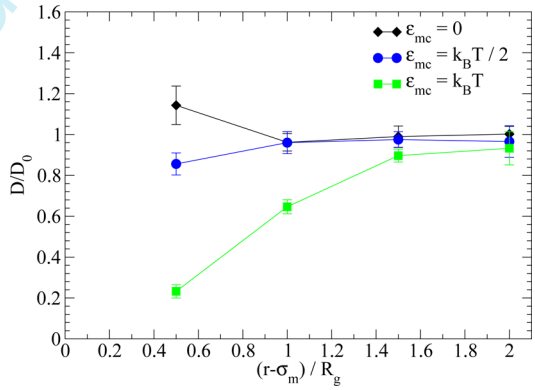

Figure 5. Self-diffusion coefficient of polymer chains (N = 60) in a monodisperse polymer melt with a SWCNT (r_{SWCNT} = 0.66) normalized by its melt value as a function of the distance r from the SWCNT surface to the polymer center of mass: (i) no attractive interaction between polymers and SWCNT (diamonds), (ii) attractive ($k_BT/2$) interaction between polymers and SWCNT (circles), and (iii) attractive (k_BT) interaction between polymers and SWCNT (squares). The solid lines have been added to guide the eye.

show the self-diffusion coefficient of polymer chains (N = 60) normalized by its melt value as a function of the radial distance r of the polymer center of mass from the SWCNT surface, for different interaction strengths of 0, $k_BT/2$ and k_BT. The interaction strength between the polymer chains and the nanotube surface affects the polymer chain diffusivity at the different shells. In particular, if there is no attractive interaction

between the polymer and the SWCNT surface ($\epsilon_{mc} = 0$), the polymer chain diffusivity is slightly enhanced in the first layer ($0 \leq r - \sigma_m < R_g/2$). In the next shells, the diffusivity regains its bulk value within the error of the simulation. In the case of weak interaction between polymers and SWCNT surface ($k_BT/2$), the polymer chain diffusivity, in the first layer, is reduced. In next shells, similarly to the $\epsilon_{mc} = 0$ case, it regains its bulk value within the error margin. A further increase in the interaction strength causes the dynamics of the first layer to slow down drastically, by about 80%, in agreement with simulation[26,31] and experimental[76−79] results from spherical nanoparticle composites and polymer melt at attractive surfaces.[80] In the shell at a distance of ($R_g + \sigma_m$) from the SWCNT surface, the polymer chain diffusivity is reduced by almost 35% from its melt value. Only at a large distance ($r = 2R_g + \sigma_m$) from the nanotube surface the polymer chains regain a bulk value within an error margin. In addition, the increase of the interaction between polymers and nanotube surface increases the distance at which the polymer chain diffusivity recovers its bulk value.

C. Effect of SWCNT Radius on Polymer Chain Dynamics. By increasing the radius of the SWCNT at a constant volume fraction, the surface area to volume ratio of the SWCNT decreases. Hence, the relative number of monomer-surface contacts decreases, and also a smaller interfacial area is formed around the nanotube surface.[12,52] As can been seen from Figure 6, (D/D_0) has a larger value for the greatest

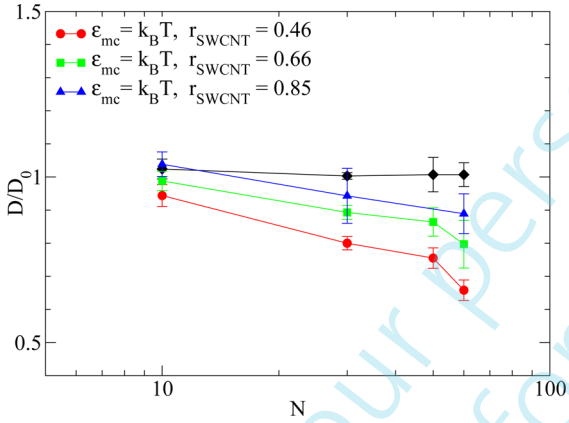

Figure 6. Self-diffusion coefficient of polymers as a function of monomers per chain in a polymer melt with a SWCNT normalized by its melt value: (i) polymer diffusion in a melt with a SWCNT without attractive interaction between polymers and SWCNT ($r_{SWCNT} = 0.66$) (diamonds), (ii) polymer diffusion in a melt with a SWCNT with attractive (k_BT) polymer/SWCNT ($r_{SWCNT} = 0.46$) interactions (circles), (iii) polymer diffusion in a melt with a SWCNT with attractive polymer/SWCNT ($r_{SWCNT} = 0.66$) interactions (squares), and (iv) polymer diffusion in a melt with a SWCNT with attractive polymer/SWCNT ($r_{SWCNT} = 0.85$) interactions (triangles). The solid lines have been added to guide the eye.

SWCNT radius ($r_{SWCNT} = 0.85$) and is comparable to the bulk value ($(D/D_0) = 1$). For the smallest SWCNT radius ($r_{SWCNT} = 0.46$), (D/D_0) is less than its bulk value (outside the error margin) for all N. For the systems of different SWCNT radii, the polymer chain diffusivity is almost similar to its bulk value in the case of the unentangled polymer chains ($N = 10$). By analogy with Figure 5, let us now discuss the dynamic behavior of the polymer chains in the different cylindrical shells around the SWCNT for different SWCNT radii, according to the position of the polymer chain center of mass. In Figure 7 we

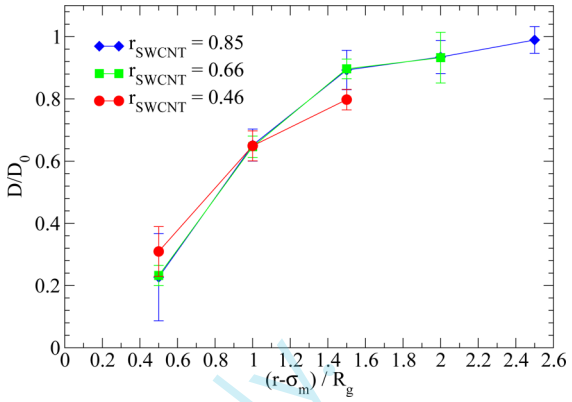

Figure 7. Self-diffusion coefficient of polymer chains ($N = 60$) with attractive (k_BT) interaction with the SWCNT in a monodisperse polymer melt with a SWCNT normalized by its melt value as a function of the distance r from the SWCNT surface: (i) $r_{SWCNT} = 0.85$ (diamonds), (ii) $r_{SWCNT} = 0.66$ (squares), and (iii) $r_{SWCNT} = 0.46$ (circles). The solid lines have been added to guide the eye.

show the self-diffusion coefficient of polymer chains ($N = 60$) normalized by its melt value as a function of the radial distance r from the SWCNT surface, for different SWCNT radii. The diffusivity of the polymer chains in all of the shells seems to be independent of SWCNT radii within the error margin. The larger nanotube radius produces a larger radius of curvature and relatively less polymer in the interfacial region.[12,81]

IV. CONCLUSIONS

The entanglements and dynamics of polymer chains in melts with and without a single embedded SWCNT were investigated by means of molecular dynamics simulations for both unentangled and entangled systems. We applied different estimators $\mathcal{N}_e(N)$ to calculate of the amount of topological constraints in our systems and extracted the N-independent entanglement length N_e. The entanglement length decreases significantly even at very low volume fractions of carbon nanotube, both with and without attractive interactions between the polymers with the SWCNT surface. This decrease of N_e in the polymer melt with SWCNT is due to the larger contour length of the primitive path, L_{pp}, that is created by the presence of the carbon nanotube. Also, we have found a dynamic heterogeneity in polymer melts in the presence of a SWCNT wherein the polymers closest to SWCNT diffuse more slowly when there is a SWCNT/polymer attraction. The overall polymer diffusion is affected by the enthalpic interaction between monomers and SWCNT for our systems for which the polymer radius of gyration exceeds the SWCNT radius. In the absence of attractive interactions between polymer chains and SWCNT, the self-diffusion coefficient of the polymer chains equals its melt value, even though the number of entanglements was found to increase. Consequently, the geometry of the SWCNT alone does not alter the polymer chain diffusion. Conversely, when the polymers are attracted to the SWCNT, there is a significant decrease of the polymer chain diffusivity, to almost zero in the vicinity of the SWCNT, when the strength of attraction dominates the thermal energy. Also, we observe a decrease of polymer chain diffusivity up to an end-to-end polymer distance away from the SWCNT surface. In addition, the polymer chain diffusivity is anisotropic with slower perpendicular diffusion to the SWCNT main axis than that parallel to it in all the entangled polymer systems with

SWCNT/polymer attraction. While our focus here has been on an isolated SWCNT work is underway to simulate the dynamics of larger systems with networks of SWCNTs.

Model Validation. *Polymer Melt Simulations – Dynamics.* In this section, we analyze the dynamic properties of polymer chains in a polymer melt for different molecular weights (Table 2) on the basis of predictions from molecular dynamics simulations. One of the simplest characterizations of the polymer melt dynamics is the self-diffusion coefficient of the polymer chains. In Figure 8 we show the product D_0N for polymers of different molecular weight.

Obviously, two different regimes can be distinguished. In the first regime, the D_0N is independent of N, and this is denoted as the Rouse[23] regime, $D_0 = D_R$. Above a certain threshold, the D_0N follows the relation

$$D_0N \propto \frac{1}{N} \tag{7}$$

It is well-known that long polymer chains follow reptation model dynamics, and their diffusion coefficient dependence on N follows the relation $D_0 \propto N^{-2}$.[13−16] As can be seen from Figure 7 the diffusion coefficient calculations from the simulations of the coarse grained model used in this study agree with the N^{-2} scaling law. In the inset of Figure 8, the D_0N product is scaled with the D_RN product of the Rouse regime and compared with the dynamics of a monodisperse experimental polystyrene melt system for different N/N_e ratios. We can see a very good agreement between the normalized simulation data and the experimental polystyrene diffusion for entangled polymer chains. In addition, there is good agreement between our predictions and the simulation model of Kremer and others[20,21,66,82,83] which neglects any monomer attraction.

Table 2. Simulations of Polymer Melts[a]

N_p (polymer chains)	N (monomers)	L	$D_0 \times 10^{-4}$
512	5	14.441	153.1
256	10	14.441	73.9
256	16	16.891	47.1
128	20	14.441	33.4
192	30	18.923	20.1
64	32	13.406	21.1
72	40	15.020	13.7
96	50	17.808	9.9
96	60	18.923	7.8
72	80	18.923	4.7
64	90	18.923	3.5
45	128	18.923	1.7

[a]Number of polymer chains N_p, number of monomers N in a polymer chain, length of the cubic simulation cell L, and self-diffusion coefficient D_0 for polymer melt systems studied in the absence of SWCNT.

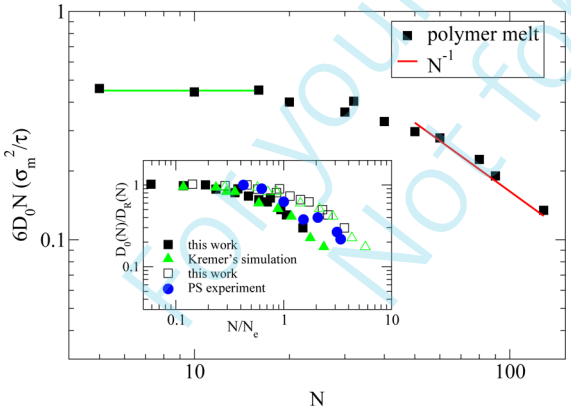

Figure 8. Product of the polymer self-diffusion coefficient with the number of monomers per polymer chain, D_0N: (i) molecular dynamics data from this work (filled squares), (ii) Rouse regime: D_RN (green line), (iii) Reptation regime: $D_0N \propto N^{-1}$ (red line). Inset: D_0N of polymer chains normalized by the corresponding D_RN of Rouse chains (N_e = 85[67,73] (filled symbols), N_e = 35[20] (open symbols)): (i) molecular dynamics data from this work (filled squares), (ii) experimental data for monodisperse polystyrene melt (PS) by Antonietti[16] (filled circles), (iii) molecular dynamics results by Kremer et al.[20,21,66,83] (open triangles).

AUTHOR INFORMATION

Corresponding Author

*E-mail: n.clarke@sheffield.ac.uk.

Notes

The authors declare no competing financial interest.

ACKNOWLEDGMENTS

This research was funded by the EPSRC/NSF Materials Network program EP/5065373/1 (EPSRC: N.C., A.K.) and DMR-0908449 (NSF: K.I.W., R.J.C.).

REFERENCES

(1) Du, F.; Scogna, R. C.; Zhou, W.; Brand, S.; Fischer, J. E.; Winey, K. I. *Macromolecules* **2004**, *37*, 9048.
(2) Hough, L. A.; Islam, M. F.; Janmey, P. A.; Yodh, A. G. *Phys. Rev. Lett.* **2004**, *93*, 1681021.
(3) Schadler, L. S.; Brinson, L. C.; Sawyer, W. G. *JOM* **2007**, *59*, 53.
(4) Moniruzzaman, M.; Winey, K. I. *Macromolecules* **2006**, *39*, 5194.
(5) Winey, K. I.; Vaia, R. A. *MRS Bull.* **2007**, *32*, 314.
(6) Winey, K. I.; Kashiwagi, T.; Mu, M. F. *MRS Bull.* **2007**, *32*, 348.
(7) Mu, M.; Clarke, N.; Composto, R. J.; Winey, K. I. *Macromolecules* **2009**, *42*, 7091.
(8) Mu, M.; Composto, R. J.; Clarke, N.; Winey, K. I. *Macromolecules* **2009**, *42*, 8365.
(9) Grady, B. P.; Paul, A.; Peters, J. E.; Ford, W. T. *Macromolecules* **2009**, *42*, 6152.
(10) Simoes, R.; Silva, J.; Vaia, R.; Sencadas, V.; Costa, P.; Gomes, J.; Lanceros-Mendez, S. *Nanotechnology* **2009**, *20*, 035703.
(11) Kumar, S. K.; Krishnamoorti, R. *Annu. Rev. Chem. Biomol. Eng.* **2010**, *1*, 37.
(12) Karatrantos, A.; Clarke, N. *Soft Matter* **2011**, *7*, 7334.
(13) Green, P. F.; Mills, P. J.; Palmstrom, C. J.; Mayer, J. W.; Kramer, E. J. *Phys. Rev. Lett.* **1984**, *53*, 2145.
(14) Green, P. F.; Kramer, E. J. *Macromolecules* **1986**, *19*, 1108.
(15) Green, P. F.; Kramer, E. J. *J. Mater. Res.* **1986**, *1*, 202.
(16) Antonietti, M.; Folsch, K. J.; Sillescu, H. *Makromol. Chem.* **1987**, *188*, 2317.
(17) Doi, M.; Edwards, S. F. *The Theory of Polymer Dynamics*; Clarendon Press: Oxford, 1986.
(18) Graessley, W. W. *Adv. Polym. Sci.* **1982**, *47*, 67.
(19) Lodge, T. P. *Phys. Rev. Lett.* **1999**, *83*, 3218.
(20) Kremer, K.; Grest, G. S. *J. Chem. Phys.* **1990**, *92*, 5057.
(21) Pütz, M.; Kremer, K.; Grest, G. S. *Europhys. Lett.* **2000**, *49*, 735.
(22) Flory, P. *Statistical Mechanics of Chain Molecules*; Hanser: New York, 1969.
(23) Rubinstein, M.; Colby, R. H. *Polymer Physics*; Oxford University Press: New York, 2003.
(24) Vacatello, M. *Macromolecules* **2001**, *34*, 1946.

(25) Ozmusul, M. S.; Picu, R. C. *Polymer* **2002**, *43*, 4657.
(26) Smith, G. D.; Bedrov, D.; Li, L.; Byutner, O. *J. Chem. Phys.* **2002**, *117*, 9478.
(27) Brown, D.; Mele, P.; Marceau, S.; Alberola, N. D. *Macromolecules* **2003**, *36*, 1395.
(28) Desai, T.; Keblinski, P.; Kumar, S. K. *J. Chem. Phys.* **2005**, *122*, 134910.
(29) Dionne, P. J.; Osizik, R.; Picu, C. R. *Macromolecules* **2005**, *38*, 9351.
(30) Dionne, P. J.; Picu, C. R.; Ozisik, R. *Macromolecules* **2006**, *39*, 3089.
(31) Huang, J.; Mao, Z.; Qian, C. *Polymer* **2006**, *47*, 2928.
(32) Picu, R. C.; Rakshit, A. *J. Chem. Phys.* **2007**, *126*, 144909.
(33) Goswami, M.; Sumpter, B. G. *J. Chem. Phys.* **2009**, *130*, 134910.
(34) Liu, J.; Cao, D.; Zhang, L.; Wang, W. *Macromolecules* **2009**, *42*, 2831.
(35) Termonia, Y. *J. Polym. Sci., Part B: Polym. Phys.* **2010**, *48*, 687.
(36) Goswami, M.; Sumpter, B. G. *Phys. Rev. E* **2010**, *81*, 041801.
(37) Liu, J.; Wu, Y.; Shen, J.; Gao, Y.; Zhang, L.; Cao, D. *Phys. Chem. Chem. Phys.* **2011**, *13*, 13058.
(38) Ndoro, T. V. M; Böhm, M. C.; Muller-Plathe, F. *Macromolecules* **2012**, *45*, 171.
(39) Borodin, O.; Bedrov, D.; Smith, G. D.; Nairn, J.; Bardenhagen, S. *J. Polym. Sci., Part B: Polym. Phys.* **2005**, *43*, 1005.
(40) Toepperwein, G. N.; Riggleman, R. A.; de Pablo, J. J. *Macromolecules* **2011**, *45*, 543.
(41) Starr, F. W.; Schrøder, T. B.; Glotzer, S. C. *Phys. Rev. E* **2001**, *64*, 021802.
(42) Starr, F. W.; Schrøder, T. B.; Glotzer, S. C. *Macromolecules* **2002**, *35*, 4481.
(43) Li, Y.; Kröger, M.; Liu, W. K. *Macromolecules* **2012**, *45*, 2099.
(44) Smith, J. S.; Bedrov, D.; Smith, G. D. *Compos. Sci. Technol.* **2003**, *63*, 1599.
(45) Zeng, Q. H.; Yu, A. B.; Lu, G. Q. *Prog. Polym. Sci.* **2008**, *33*, 191.
(46) Wei, C.; Srivastava, D.; Cho, K. *Nano Lett.* **2002**, *2*, 647.
(47) Liu, J.; Wang, X. L.; Zhao, L.; Zhang, G.; Lu, Z. Y.; Li, Z. S. *J. Polym. Sci., Part B: Polym. Phys.* **2008**, *46*, 272.
(48) Wu, C. *J. Polym. Sci., Part B: Polym. Phys.* **2011**, *49*, 1123.
(49) Yang, J.-S.; Yang, C.-L.; Wang, M.-S.; Chen, B.-D.; Ma, X.-G. *Phys. Chem. Chem. Phys.* **2011**, *13*, 15476.
(50) Li, Y. *Polymer* **2011**, *52*, 2310.
(51) Peter, S.; Meyer, H.; Baschnagel, J. *Eur. Phys. J. E: Soft Matter Biol. Phys.* **2009**, *28*, 147.
(52) Karatrantos, A.; Composto, R. J.; Winey, K. I.; Clarke, N. *Macromolecules* **2011**, *44*, 9830.
(53) Bennemann, C.; Paul, W.; Binder, K. *Phys. Rev. E* **1998**, *57*, 843.
(54) Allen, M. P.; Tildesley, D. J. *Computer Simulation of Liquids*; Clarendon Press: Oxford, 1987.
(55) Frenkel, B.; Smit, D. *Understanding Molecular Simulation: From Algorithms to Applications (Computational Science)*; Academic Press: 1996.
(56) Bekker, H.; Berendsen, H. J. C.; Dijkstra, E. J.; Achterop, S.; van Drunen, R.; van der Spoel, D.; Sijbers, A.; Keegstra, H.; Reitsma, B.; Renardus, M. K. R. *Physics Computing* **1993**, *92*, 252.
(57) Berendsen, H. J. C.; van der Spoel, D.; van Drunen, R. *Comput. Phys. Commun.* **1995**, *91*, 43.
(58) Lindahl, E.; Hess, B.; van der Spoel, D. *J. Mol. Model.* **2001**, *7*, 306.
(59) van der Spoel, D.; Lindahl, E.; Hess, B.; Groenhof, G.; Mark, A.; Berendsen, H. *J. Comput. Chem.* **2005**, *26*, 1701.
(60) Frankland, S. J. V.; Harik, V. M.; Odegard, G. M.; Brenner, D. W.; Gates, T. S. *Compos. Sci. Technol.* **2003**, *63*, 1655.
(61) Peter, S.; Meyer, H.; Baschnagel, J. *J. Polym. Sci., Part B: Polym. Phys.* **2006**, *44*, 2951.
(62) Hoover, W. G. *Phys. Rev. A* **1985**, *31*, 1695.
(63) Nosé, S. *Mol. Phys.* **1984**, *52*, 255.
(64) Hockney, R. W.; Goel, S. P.; Eastwood, J. *J. Comput. Phys.* **1974**, *14*, 148.
(65) Auhl, R.; Everaers, R.; Grest, G. S.; Kremer, K.; Plimpton, S. J. *J. Chem. Phys.* **2003**, *119*, 12718.
(66) Everaers, R.; Sukumaran, S. K.; Grest, G. S.; Svaneborg, C.; Sivasubramanian, A.; Kremer, K. *Science* **2004**, *303*, 823.
(67) Hoy, R. S.; Foteinopoulou, K.; Kröger, M. *Phys. Rev. E* **2009**, *80*, 031803.
(68) Kröger, M. *Comput. Phys. Commun.* **2005**, *168*, 209.
(69) Shanbhag, S.; Kröger, M. *Macromolecules* **2007**, *40*, 2897.
(70) Karayiannis, N. C.; Kröger, M. *Int. J. Mol. Sci.* **2009**, *10*, 5054.
(71) Sukumaran, S. K.; Grest, G. S.; Kremer, K.; Everaers, R. *J. Pol. Sci., Part B: Polym. Phys.* **2005**, *43*, 917.
(72) Uchida, N.; Grest, G. s.; Everaers, R. *J. Chem. Phys.* **2008**, *128*, 044902.
(73) Hou, J. X.; Svaneborg, C.; Everaers, R.; Grest, G. S. *Phys. Rev. Lett.* **2010**, *105*, 068301.
(74) Meyer, H.; Kreer, T.; Cavallo, A.; Wittmer, J. P.; Baschnagel, J. *Eur. Phys. J. Special Topics* **2007**, *141*, 167.
(75) Vladkov, M.; Barrat, J. L. *Macromolecules* **2007**, *40*, 3797.
(76) Kropka, J.; Pütz, K. W.; Pryamitsyn, V.; Ganesan, V.; Green, P. F. *Macromolecules* **2007**, *40*, 5424.
(77) Kropka, J. M.; Sakai, V. G.; Green, P. F. *Nano Lett.* **2008**, *8*, 1061.
(78) Harton, S. E.; Kumar, S. K.; Yang, H. C.; Koga, T.; Hicks, K.; Lee, E.; Mijovic, J.; Liu, M.; Vallery, R. S.; Gidley, D. W. *Macromolecules* **2010**, *43*, 3415.
(79) Chen, L.; Zheng, K.; Tian, X.; Hu, K.; Wang, R.; Liu, C.; L. Y.; Cui, P. *Macromolecules* **2010**, *43*, 1076.
(80) Smith, G. D.; Bedrov, D.; Borodin, O. *Phys. Rev. Lett.* **2003**, *90*, 226103.
(81) Schadler, L. *Nat. Mater.* **2007**, *6*, 257.
(82) Kröger, M.; Loose, W.; Hess, S. *J. Rheol.* **1993**, *37*, 1057.
(83) Kremer, K.; Sukumaran, S. K.; Everaers, R.; Grest, G. S. *Comput. Phys. Commun.* **2005**, *169*, 75.